Subpixel burn detection in Moderate Resolution Imaging Spectroradiometer 500-m data with ARTMAP neural networks

N. V. Shabanov, K. Lo, S. Gopal, and R. B. Myneni
Department of Geography, Boston University, Boston, Massachusetts, USA

Received 20 July 2004; revised 24 October 2004; accepted 18 November 2004; published 9 February 2005.

[1] This paper presents an ARTMAP neural network approach for burn detection in Moderate Resolution Imaging Spectroradiometer (MODIS) data using two methods: discrete and continuous classifications. The study area covers the states of Idaho and Montana in the United States, where extensive fire events took place during the months of July and August in the year 2000. The proposed approach differs from commonly used change detection schemes by utilizing a single surface reflectance image instead of time series of satellite data. Burn detection in this study was accomplished by the classification of land into four classes: burns, woody vegetation, herbaceous vegetation, and barren. We performed the discrete classification of coarse (500-m MODIS data) and high-resolution (30-m Enhanced Thematic Mapper (ETM+) data) surface reflectance data with an ARTMAP classifier to evaluate the impact of a land cover mixture on burn detection. The analysis of classification results reveals commission and omission errors in the evaluation of burn area extent at a coarse-resolution scale. To account for land cover heterogeneity, we utilized the continuous classification of coarse-resolution data with an ARTMAP mixture model. A training data set on the land cover mixture at 500-m scale of MODIS data was assembled from the aggregated 30-m ETM+ classification. The ARTMAP mixture model was trained with MODIS surface reflectance data and land cover mixture information to generate a continuous classification of burns (expressed in percentage of burns per pixel). Data fusion of coarse- and high-resolution satellite data in this study resulted in a more natural and accurate mapping of burns as mixtures with other land cover types.

Citation: Shabanov, N. V., K. Lo, S. Gopal, and R. B. Myneni (2005), Subpixel burn detection in Moderate Resolution Imaging Spectroradiometer 500-m data with ARTMAP neural networks, *J. Geophys. Res.*, *110*, D03111, doi:10.1029/2004JD005257.

1. Introduction

[2] Biomass burning is a major cause of Earth's land cover conversion. Fires destruct natural ecosystems, deposit ash on the ground, and release land surface carbon stocks to the atmosphere, which alters biosphere-atmosphere interactions at regional and global scales [*Levine et al.*, 1995; *Scholes*, 1995; *Sellers et al.*, 1995]. Changes of ground characteristics (such as surface albedo, evapotranspiration, surface roughness) and atmospheric composition (emission of trace gases and smoke aerosols) alter the Earth's radiation budget and introduce uncertainties in climate modeling. Accurate and timely accounting of burns is critical for the management of natural resources and the monitoring of biodiversity and animal habitat.

[3] Ground monitoring of fires and burned areas is mostly performed by agencies at regional scale (site 1 in Table 1) and has limitation on accuracy, spatial coverage, temporal frequency of the update on the event status and associated costs. Satellite remote sensing provides an optimal alternative way of monitoring fires and burned areas at regional and especially at global scales. Currently, remote sensing of fires is a well-established technology based on the hot spot detection in satellite sensor mid IR and thermal IR channels. Several global fire products are currently in operational production including Global Fire Atlas from European Space Agency (ESA) Along Track Scanning Radiometer (ATSR) [*Arino et al.*, 2001] and fire product from National Aeronautic and Space Administration's (NASA) Moderate resolution Imaging Spectroradiometer (MODIS) [*Justice et al.*, 2002].

[4] In contrast to fire detection, the selection of an optimal technology for burn detection is ongoing research. In general, RED, NIR, and SWIR channels and normalized difference vegetation index (NDVI) are selected for burn mapping in the framework of a change detection scheme. *Kasischke and French* [1995] used the drop in NDVI 1-km data from National Oceanic and Atmospheric Administration's (NOAA) advanced very high resolution radiometer (AVHRR) to map burns in Alaska. *Eva and Lambin* [1998] utilized the raise in surface temperature and the decrease in SWIR reflectance data from the ATSR instrument to study burns in central Africa. *Fraser et al.* [2000] implemented a synergistic hot spot and NDVI-based algorithm for burn detection in 1-km NOAA AVHRR data over boreal forests

0148-0227/05/2004JD005257$09.00

Table 1. World Wide Web Sites

Organization/Sponsor	Site Number	Access Address
National Interagency Fire Center	1	http://www.nifc.gov
MOD09A1 user guide	2	http://modis-land.gsfc.nasa.gov/MOD09/MOD09ProductInfo/MOD09_L3_8-day.htm
MOD12Q1 user guide	3	http://geography.bu.edu/landcover/userguidelc/lc.html
MOD14A2 user guide	4	http://modis-fire.gsfc.nasa.gov/methodology.asp
ATSR-1 User Guide	5	http://www.atsr.rl.ac.uk/documentation/docs/userguide/index.shtml
Landsat 7, user handbook	6	http://ltpwww.gsfc.nasa.gov/IAS/handbook/handbook_toc.html
Idaho 30-m land cover from GAP	7	ftp://ftp.gap.uidaho.edu/products/idaho/gis/landcover/
Montana Department of Nature Resources and Conservation Forestry division	8	http://www.dnrc.state.mt.us/forestry
MODIS vegetation continuous fields land cover	9	http://glcf.umiacs.umd.edu/data/modis/vcf/

in Canada. *Roy et al.* [2002] utilized changes in MODIS nadir SWIR surface reflectances data at 500-m resolution to monitor burns in South Africa. *Zhan et al.* [2002] developed an algorithm in the framework of the MODIS Vegetation Cover Conversion (VCC) project for global burn detection in MODIS 250-m data from the analysis of changes in RED-NIR spectral signatures of different land cover types. *Brivio et al.* [2003] performed a MultiLayer Perception neural network classification of RED, NIR and SWIR 1.1- to 1.7-km data from le Système pour l'Observation de la Terre, the VEGETATION (SPOT-VGT) sensor to map burns in northern Africa.

[5] The application of a change detection approach to burn mapping is complicated by variations in surface reflectances as function of Sun-target-sensor geometries (BRDF effect), variations in the accuracy of atmospheric correction as function of image acquisition time, variations in geolocation errors, problem of separation of phenological changes from those due to biomass burning, lack of temporal persistence of burns (vegetation regrowth) and others [*Brivio et al.*, 2003; *Roy et al.*, 2002]. Several methods were designed to alleviate these problems: compositing data to reduce the threshold sensitivity to bidirectional reflectance effects and residual cloud and atmospheric contamination, and application of empirical correction factors to account for phenological changes in vegetation [*McDonald et al.*, 1998; *Zhan et al.*, 1998; *Roy et al.*, 2002]. An alternative approach to burn detection is to use a single satellite image (instead of time series of data) and search directly for spectral signatures of burns. This approach has the advantage of decreasing the amount of data processing (a single image versus time series of images) which is especially useful for real-time applications, as well as reducing the other problems highlighted above. The research presented here implements this strategy with atmospherically corrected surface reflectance data at 500-m spatial resolution recorded by MODIS on board of the EOS Terra platform for burns detection with the ARTMAP supervised classification [*Carpenter et al.*, 1999a]. At the scale of spatial resolution of MODIS data, burns often occur as mixtures with other land cover types. The mixture of land cover types introduces uncertainties in training of the ARTMAP classification algorithm, which translates into commission/omission classification errors. Therefore we utilized the ARTMAP mixture model [*Carpenter et al.*, 1999b] to characterize subpixel burns at coarse spatial resolution. The training of the ARTMAP mixture model was performed based on the mixture information derived from the high-resolution imagery (30-m ETM+ data).

[6] This paper is organized as follows. In section 2, we describe the study area, provide a summary of satellite data sources used in the project, and give background information on the ARTMAP classifier and the ARTMAP mixture model. In section 3, we describe a procedure of ARTMAP training for burn detection from the discrete classification, present results of the classification of MODIS and ETM+ data, and compare burns detected in MODIS data with MODIS and ATSR fire products. Additionally, the impact of land cover heterogeneity on burn detection from coarse-resolution MODIS surface reflectance data is analyzed on the basis of the classification of high-resolution ETM+ data. Section 4 introduces an approach to MODIS subpixel burn area mapping with the ARTMAP mixture model. The conclusions are summarized in the last section.

2. Data and Algorithms

2.1. Data

[7] In this study we focus on burn detection after a fire event in the northwestern region of the United States (Idaho and Montana, July–August 2000). In Idaho alone, there was more than 500,000 acres of forest that burned during the peak fire season in the Payette National Forest and Salmon National Forest (site 1 in Table 1). This fire event defined the selection of spatial and temporal coverage of satellite data for the analysis. The research presented in this paper utilizes data products from three satellite sensors: surface reflectances, land cover and fire products from the MODIS sensor onboard the Terra platform, surface reflectances from the ETM+ sensor onboard the Landsat 7 platform, and fire product from the ATSR-1 and ATSR-2 sensors onboard the ERS-2 platform. The MODIS scene covers a spatial region specified by its four corners (lat/long) as follows: upper left (UL) = 49.988°/−139.959°, lower left (LL) = 39.996°/−117.463°, lower right (LR) = 39.996°/−104.421°, upper right (UR) = 49.988°/−124.419°. The corresponding coordinates for the ETM+ scene are: UL = 45.594249°/−116.7410135°, LL = 43.6389180°/−116.7495622°, LR = 43.5918191°/−113.7097746°, UR = 45.5438482°/−113.5977207°. The MODIS scene contains 2400 samples × 2400 lines = 5,760,000 pixels, while the ETM+ scene has 8181 samples × 7241 lines = 59,238,621 pixels. Below we provide a short summary for each data product used.

[8] The MODIS surface reflectances MOD09A1 product, is an 8-day composite product of daily MODIS surface reflectance data for seven spectral land bands at 500-m spatial resolution (site 2 in Table 1). The product is an

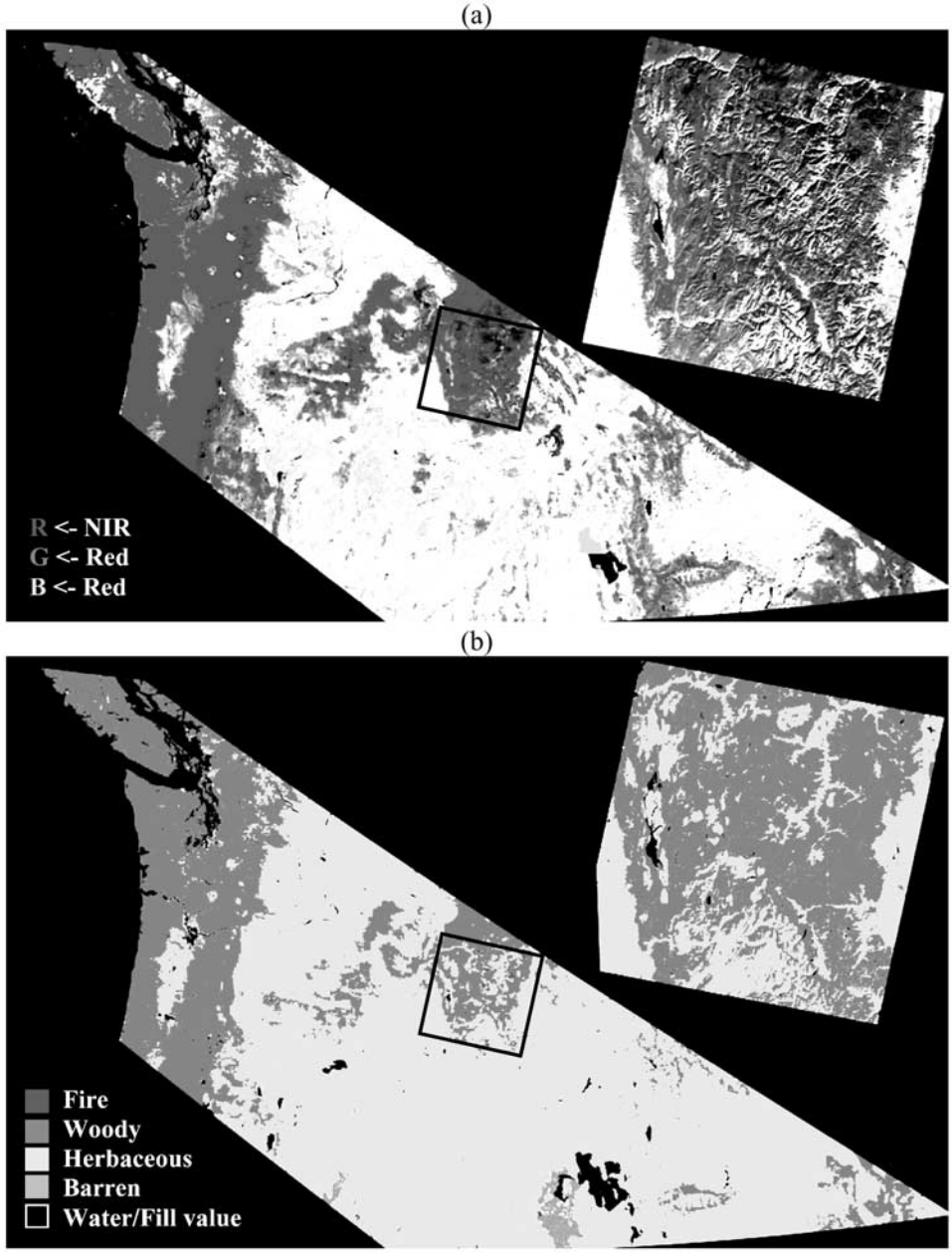

Figure 1. Input data for burn detection with the ARTMAP neural network. (a) The Moderate Resolution Imaging Spectroradiometer (MODIS) 8-day composite surface reflectance product at 500-m spatial resolution for 5–12 September 2000, tile h09v04 (h indicates horizontal; v indicates vertical), reprojected to the universal transverse Mercator (UTM) projection. (inset) Enhanced Thematic Mapper (ETM+) surface reflectance data at 30-m spatial resolution for 8 October 2000, path 41/row 29, the UTM projection. (b) The three vegetation life forms land cover for the above–MODIS tile overlaid with the composite (20 August to 12 September 2000) of MODIS fire product. (inset) Three vegetation life forms land cover for the ETM+ scene. See color version of this figure at back of this issue.

estimate of the surface spectral reflectance for each band as it would have been measured at ground level if there were no atmospheric scattering or absorption [*Vermote et al.*, 1997, 2002]. Research utilizes RED (620–670 nm) and NIR (841–876 nm) bands only. We selected the collection 3 surface reflectance product for MODIS tile h09v04, 5–12 September 2000 composite (Figure 1a).

[9] The MODIS land cover, MOD12Q1 product, provides land cover at four classification schemes, including the International Geosphere-Biosphere Programme (IGBP) scheme, at spatial resolution of 1 km [*Friedl et al.*, 2002] (site 3 in Table 1). We utilized the collection 3 product for MODIS tile h09v04, generated based on 1 year of MODIS data (15 October 2000 through 15 October 2001). The 17-class IGBP classification was cross walked to a three-vegetation life form classification (see section 3.1) for the purpose of our analysis (Figure 1b).

[10] The MODIS fire and thermal anomalies, MOD14A2 product, is an 8-day composite product at 1-km spatial resolution [*Justice et al.*, 2002] (site 4 in Table 1). The hot spot detection algorithm utilizes two mid IR (3929–3989 nm) and one thermal IR (10,780–11,280 nm) MODIS bands to derive the likelihood of fire and hot objects on the surface. Additionally, for daytime observations, it incorporates the MODIS RED and NIR bands to filter out a false-positive fire signal due to possible Sun glint contamination. We utilized the collection 3 product for MODIS tile h09v04. The temporal compositing of this product for 20 August through 12 September of year 2000 was performed in this research to cover the majority of fire events in the study area.

[11] The ATSR fire product, Global Fire Atlas, is a monthly composite product, at spatial resolution of 1 km (site 5 in Table 1). The fire detection algorithm uses the ATSR-1 and ATSR-2 mid IR channel (3550–3930 nm) to detect a hot spot. The algorithm uses only nighttime data as an input to prevent false fire detection due to Sun glints. For each hot spot detected, this product records its date, time, latitude and longitude. We utilized Global Fire Atlas data for the month of August in year 2000 over the spatial extent of MODIS tile h09v04.

[12] The ETM+ top of atmosphere reflectances product provides radiometrically and geometrically corrected data (site 6 in Table 1). Our research utilizes RED (630–690 nm) and NIR (760–900 nm) bands only. We selected the ETM+ scene for path 41/row 29, acquired on 8 October 2000. Atmospheric correction was performed in this research based on the dark target method to convert top of the atmosphere reflectances to the surface reflectances (Figure 1a).

[13] The Idaho 30-m land cover was created under the Gap Analysis Program (GAP) project (site 7 in Table 1). This land cover is a compilation of the Current Vegetation Map of northern Idaho/western Montana and the Idaho/western Wyoming land cover classification. Both sources use primarily 1992 and 1993 satellite imagery acquired during the growing season (June–September). These classifications were cross walked and merged to produce a unified land cover map for Idaho. The GAP land cover classification was cross walked to the three vegetation life form classification (see section 3.1) for the purpose of our analysis (Figure 1b).

[14] Consider several additional remarks on our choice of data sources. The proposed burn detection technique utilizes RED and NIR channel data only. However, according to the literature (see section 1), SWIR channels were also found quite sensitive to burns. Our research on the performance of ARTMAP with MODIS data indicates highly correlated spatial distribution of detected patterns of burns in forested regions for NIR and SWIR input data. RED data are less sensitive to burns. Selection of both RED and NIR channels provided several advantages to our research. First, RED and NIR data are optimal for vegetation mapping, and therefore required for the evaluation of a mixture of vegetation and burns. Second, RED and NIR data are available from the MODIS sensor at a variety of spatial resolutions (250 m, 500 m and 1 km) while this is not the case for SWIR data. For instance, our approach can be extended to MODIS 250-m data, a valuable source for mixture analysis, but only RED and NIR data are available at this scale. The final comment is on the potential impact of the difference in the acquisition times between the MODIS and the ETM+ images (5 September and 8 October 2000, respectively) on burn detection. One month difference in image acquisition times is due to our restrictions on the selection of MODIS and ETM+ images with minimum cloud cover. Given the fire event timing (July–August 2000), data from both sensors should capture the same burns. Also, vegetation regrowth is negligible during one month in the fall season at forested regions. However, in general, vegetation regrowth should be considered for burn detection over regions with a high rate of regrowth, such as savanna.

2.2. ARTMAP Classifier

[15] The family of ARTMAP neural network systems has been developed by researchers at Boston University and was applied in multiple areas of land remote sensing: land cover mapping [*Gopal et al.*, 1999; *Carpenter et al.*, 1999a], mixture modeling [*Carpenter et al.*, 1999b], change detection [*Abuelgasim et al.*, 1999], and efficient mapping [*Carpenter et al.*, 1999a]. In this study, a fuzzy ARTMAP version [*Carpenter et al.*, 1992; *Carpenter*, 1997] is used in the application of burns detection. The basic building block of the fuzzy ARTMAP supervised classification system is a fuzzy ART module, unsupervised learning network. Pattern recognition performed by this module is based on the adaptive resonance theory [*Grossberg*, 1976] and incorporates the fuzzy logic for set theoretical operations [*Zadeh*, 1965]. The ART module is a two-level network of interconnected nodes: a comparison level (F_1) and a recognition level (F_2). An input signal is first recorded by F_1 node and propagated to F_2 level, where a single node (category) is activated. Activated F_2 node sends its signal back to F_1 level, where it is compared with the original input. If the two patterns are close according to the vigilance parameter, ρ, a resonance occurs and long-term memory is altered to incorporate a new observation. If the two patterns are different, ART module searches F_2 level until matching F_2 category is found; otherwise, a new category is established.

[16] The fuzzy ARTMAP system consist of a pair of fuzzy ART modules (ART_a and ART_b), connected by the associative learning network (map field) and the internal controller (Figure 2). The controller creates a minimum number of ART_a recognition categories (“hidden units”), needed to meet the accuracy criteria. ARTMAP automatically links predictive success to the category size by increasing the ART_a vigilance parameter $\rho = \rho_a$ by the minimal amount needed to correct a predictive error at ART_b. A high level of vigilance (over 0.7) will lead to a better discrimination of classes as the network holds a larger amount of internal categories, while a low vigilance level will generally lead to a coarse categorization [*Carpenter et al.*, 1999a]. This study uses vigilance of 0. During supervised training, ART_a receives a stream of patterns a(n) and ART_b receives a stream of patterns b(n), where b(n) is a correct prediction given a(n). The two modules classify a(n) and b(n) into categories and the map field makes the association between ART_a and ART_b categories. Owing to the noise in training data set and other factors, different ordering of the input set causes different class predictions. The voting process allows for

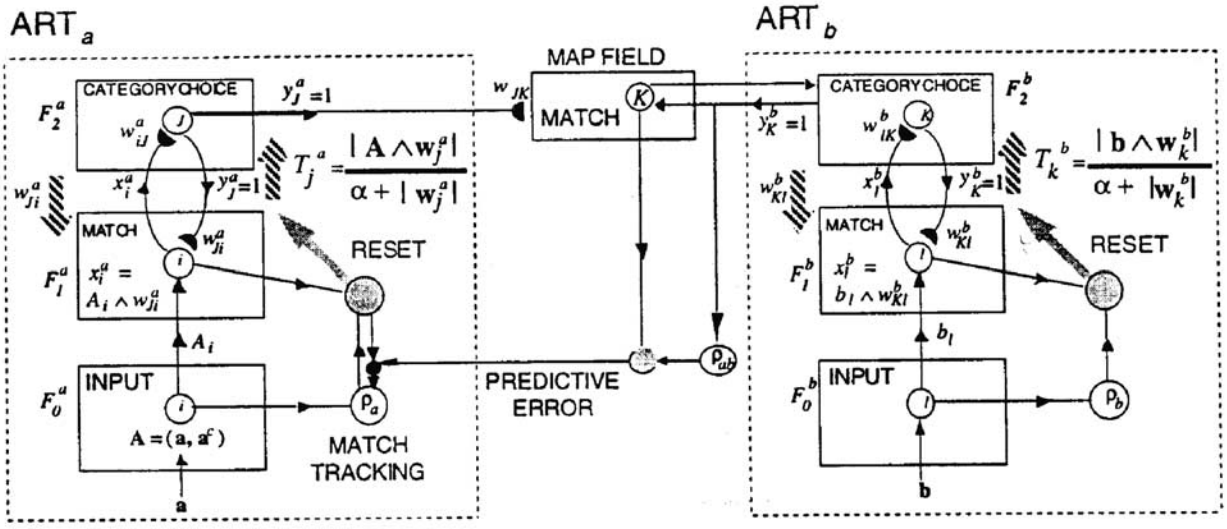

Figure 2. Fuzzy ARTMAP architecture. Reprinted from *Carpenter et al.* [1999b], with permission from Elsevier.

combining results from multiple predictions. This approach has two advantages: (1) It can improve the classification accuracy [*Carpenter*, 1997]; (2) it provides a way for evaluating uncertainty in the results on a pixel-by-pixel basis. This study uses five voters. To characterize uncertainties in burn detection, ARTMAP outputs primary and secondary images, which were used in this study to identify the lower and upper approximation of burns extent for the discrete classification.

2.3. ARTMAP Mixture Model

[17] During the recent decade, extensive research has been performed for subpixel land cover characterization. Several approaches were implemented, including linear mixture models [*DeFries et al.*, 1999, *Hansen et al.*, 2002], neural networks [*Carpenter et al.*, 1999b], maximum likelihood classifiers [*Schowengerdt*, 1996] and decision trees [*McIver and Friedl*, 2002]. In this research, we follow the ARTMAP mixture model of *Carpenter et al.* [1999b]. This model was applied for identifying the life form components of a vegetation mixture from Landsat Thematic Mapper imagery.

[18] The training of the ARTMAP classifier and the ARTMAP mixture model is organized in a similar fashion. In both cases, ARTMAP is presented with input vectors (spectral reflectances) and expected output for the set of training pixels. In the case of the ARTMAP classifier, the output is just a predicted class (the proportion of the predicted class is 1, and the proportions of other classes are 0), while in the case of the ARTMAP mixture model, the output consists of the measured proportions for each class for a particular training pixel. The training strategy of the ARTMAP mixture model is different from the training of the linear mixture model, which is based on the sampling of pure classes (end-members). Owing to the significant variability of optical properties even within one class, end-members are selected with uncertainties which affect the classification accuracy [*Carpenter et al.*, 1999b]. The experience with the ARTMAP mixture model suggests improvements in classification results, when sampling the variability of mixture proportions for each class [*Carpenter et al.*, 1999b]. The benefit of a complex training procedure is that the ARTMAP mixture model is able to capture the nonlinear relationship between the proportions of classes and the location of surface reflectances corresponding to these mixtures in the spectral space [*Carpenter et al.*, 1999b]. This results in better performance in terms of classification accuracy. In addition, the linear mixture model can retrieve only n+1 class, where n is the number of input vectors, while this restriction is not required by the ARTMAP mixture model.

3. Burn Detection From the Discrete Classification of MODIS Surface Reflectance Data

[19] This section details the discrete classification approach to burns mapping from MODIS coarse-resolution surface reflectance data with the ARTMAP neural network. The proposed burn detection technique utilizes single satellite images, in contrast to the requirements of the change detection scheme. Detected burns were compared with fire product from the MODIS and the ATSR sensors. Additionally, we performed burn detection in high-resolution satellite data (ETM+ surface reflectances) and compared results with MODIS burns retrievals to evaluate the impact of a land cover mixture on burn detection in coarse-resolution data.

Table 2. Cross Walking From the MODIS IGBP Land Cover to the Three Vegetation Life Forms[a]

Three Life Forms	IGBP Class Labels
Woody	evergreen needleleaf forest, evergreen broadleaf forest, deciduous needleleaf forest, deciduous broadleaf forest, mixed forests, closed shrublands, and woody savannas
Herbaceous	open shrublands, savannas, grasslands, croplands, and croplands/natural vegetation mosaic
Bare	barren or sparsely vegetated

[a]MODIS is Moderate Resolution Imaging Spectroradiometer; IGBP is International Geosphere-Biosphere Programme.

Table 3. Cross Walking From the GAP Land Cover Classification for the States of Idaho/Montana to the Three Vegetation Life Forms

Three Life Forms	Idaho/Wyoming Class Labels
Woody	broadleaf forest, needleleaf forest, mixed needleleaf/broadleaf forest, and standing burnt or dead timber
Herbaceous	agricultural land, grasslands, mesic shrublands, and xeric shrublands
Bare	barren lands

3.1. Training Strategy

[20] The accuracy of burn detection from the discrete classification with ARTMAP depends on the selection of spectrally distinct signatures of the class of interest (burns) and nonburn classes. We minimized the number of classes because of the restrictions on the spectral space (RED and NIR bands only) and the amount of satellite images (single image). Three classes of the vegetation life forms, woody, herbaceous, and bare, were selected to specify nonburn classes. This four class classification is sufficient for burn detection, on one hand, and allows for the extension of the method to account for the effect of land cover mixture on burns retrievals, on the other.

[21] Sampling of training data for burns in MODIS and ETM+ surface reflectance data was performed referencing MODIS fire product and ancillary sources. We aggregated available three consecutive 8-day images of MODIS fire product (20 August through 12 September 2000) to sample the majority of the active fires responsible for the burn scars at the study area. We also used ancillary information to avoid a bias due to the incomplete coverage of fire events as well as the uncertainties in the MODIS fire product. This includes compilation of ground truth data from the National Interagency Fire Center (site 1 in Table 1) and the Montana Department of Nature Resources and Conservation Forestry Division (site 8 in Table 1), as well as expert visual inspection of the input surface reflectances in the false color representation.

[22] Selection of training data for three vegetation life form classes for the MODIS scene was performed referencing the MODIS land cover product, IGBP classification cross walked into three vegetation life forms according to the rules specified in Table 2. Note that an alternative source is to directly use MODIS vegetation continuous fields (site 9 in Table 1). The predominant land cover class for the selected MODIS tile is herbaceous vegetation (69% out of land pixels), followed by woody vegetation (29%) and a small fraction of barren (2%). The selection of corresponding training data for the ETM+ scene was based on cross walking the GAP land cover for the states of Idaho/Montana according to the rules specified in Table 3. For the ETM+ scene the predominant land cover class is woody vegetation (68%), while herbaceous vegetation occupies a smaller portion (31%) of the image. Note that both MODIS and ETM+ surface reflectances (Figure 1a) express contrast between RED and NIR data, which is highly correlated to the corresponding land cover maps (Figure 1b). Also, note that both MODIS and GAP land covers do not indicate unvegetated areas corresponding to the burns. In the case of the GAP land cover burns are not included, because this map was generated based on the data sources collected before the studied fire event. The MODIS land cover was generated based on 1 year of MODIS data, collected after the fire event. Vegetation regrowth during spring and summer of the year following the fire event could cause the replacement of burns with herbaceous vegetation. Lack of burns in both land cover maps has no impact on the ARTMAP performance, because the above maps were used exclusively to train the classifier for three vegetation life forms, not burns.

[23] Given the data sources to specify burn and nonburn classes, the question is, What approach should be used to select appropriate subsets of surface reflectances representative of the above classes? In this research we selected training data from the subset with the most probable locations for each class in the spectral space. Specifically, we constructed the contour plots of surface reflectance data density in the RED-NIR spectral space for each class, referencing the corresponding land cover map. The internal space of each contour includes the highest-density subset of all the data. In the case of MODIS data, the contours show clear separations between classes when the majority percentage is about 60%, while 40% is required to get the separation in the case of ETM+ data. Referencing the corresponding contour plots, spatial clusters of training data were selected from the MODIS and the ETM+ images, such that training data only sample the internal area of the corresponding contour. The training data set for the MODIS (ETM+) scene include 2813 (387) samples for woody vegetation, 15,619 (298) samples for herbaceous vegetation, 2129 (220) samples for barren, and 2453 (452) samples for burns. Figures 3a and 3b illustrate the training technique for both data sets. The differences between the spectral signatures of classes for the two sensors are due to several reasons. First, both images were acquired during fall season but with a delay of approximately one month (5–12 September 2000 versus 8 October 2000). During this time of senescence, spectral vegetation properties change significantly. Additionally, the resolution of sensors impacts the spectral signatures because of the influence of land cover mixtures at coarse resolution. Also, ETM+ and MODIS have different calibration and atmospheric correction procedures. Finally, MODIS data cover spatially a significantly larger area compared to the spatial coverage of the ETM+ scene. However, the difference in the training data is not a concern here because the goal is to establish spectral separability between land cover types, which was achieved in both cases.

[24] Given the training data for each class, ARTMAP generated corresponding decision space. Figure 3 shows the decision space for the discrete classification with ARTMAP both for the MODIS (Figure 3c) and the ETM+ (Figure 3d) data, when input vectors are restricted to the observed values of corresponding surface reflectances.

3.2. Accuracy Evaluation

[25] We performed the ARTMAP discrete classification of the MODIS scene with the above described training data. The resulting classification map (burns, woody, herbaceous and barren classes) is shown in Figure 4. Cloud contaminated pixels were excluded from the classification according to the cloud bits QA in the MOD09A1 product (site 1 in Table 1). As an initial step for accuracy assessment, we

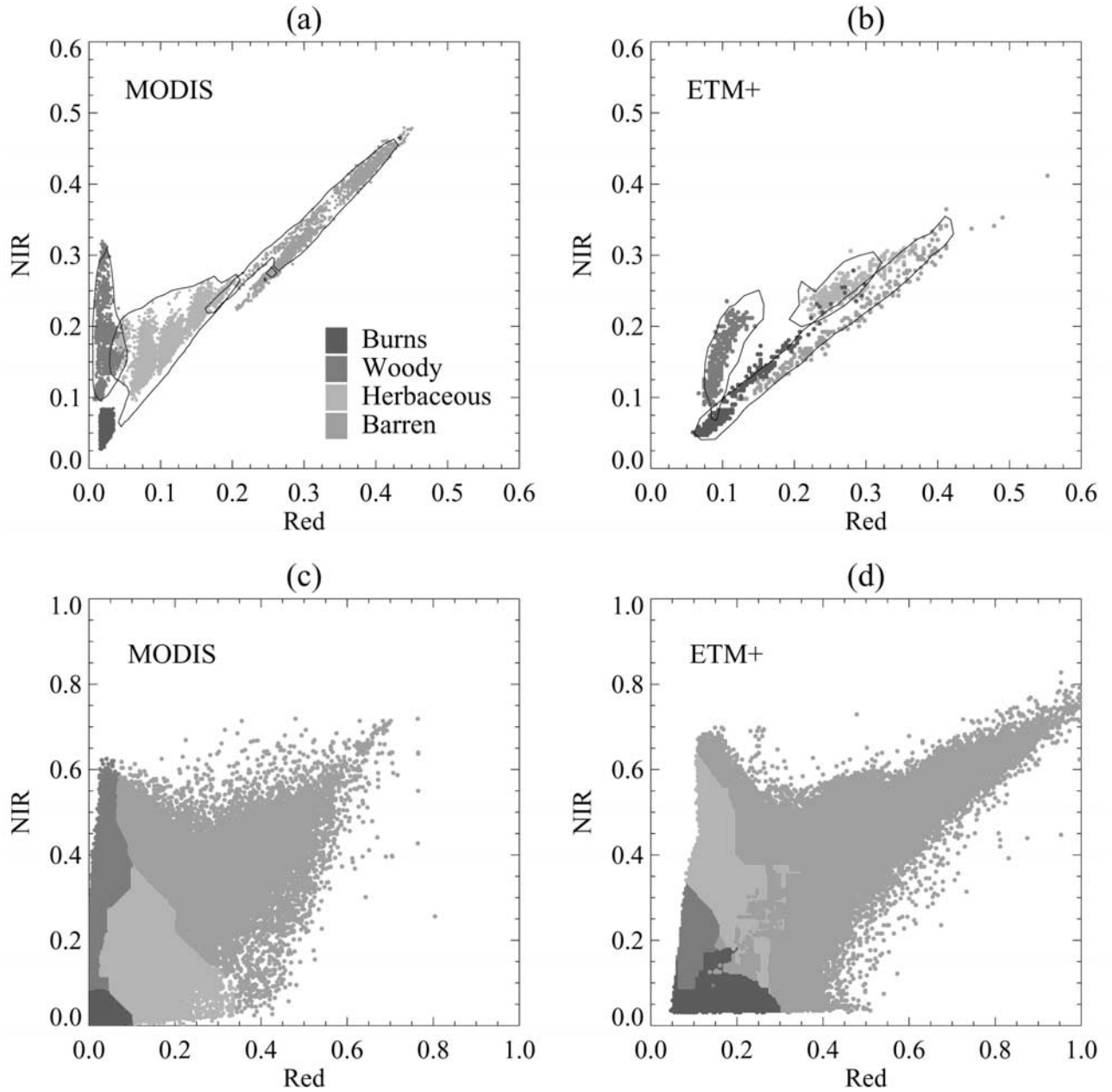

Figure 3. Selection of the training data for the discrete classification. (a) Sixty percent contour plots identifying the location of the highest density MODIS surface reflectance data in the RED-near-infrared (NIR) spectral space for the three vegetation life form and burn classes. Training data (shown as scatterplots) were randomly selected to cover the internal area (the highest data density) of the corresponding contour plots for each class. (b) Same as Figure 3a but for the ETM+ surface reflectances. Contour plots were generated at 40% level. (c) ARTMAP decision space for MODIS data. The distribution of classes is predicted by the ARTMAP in the RED and NIR spectral space when the input vectors are restricted to the observed values of surface reflectances data. (d) Same as Figure 3c but for the ETM+ data.

compared the ARTMAP classification with the MODIS land cover product cross walked to three vegetation life forms and overlaid with the MODIS fire product (Figure 1b). Upon the visual inspections of Figures 4 and 1b, one can note that the two classifications are mostly similar, with the exceptions of some herbaceous vegetation pixels that are misclassified as bare and the misclassification of woody vegetation at the lower right-hand side of the image. We performed a standard error analysis with the error matrix shown in Table 4. The overall accuracy is high, about 84.5%, which is due to the low commission/omission errors for the two predominant classes in the scene (0.29/0.25 for woody and 0.17/0.23 for herbaceous). The bare class constitutes a small portion of the scene and has a low omission

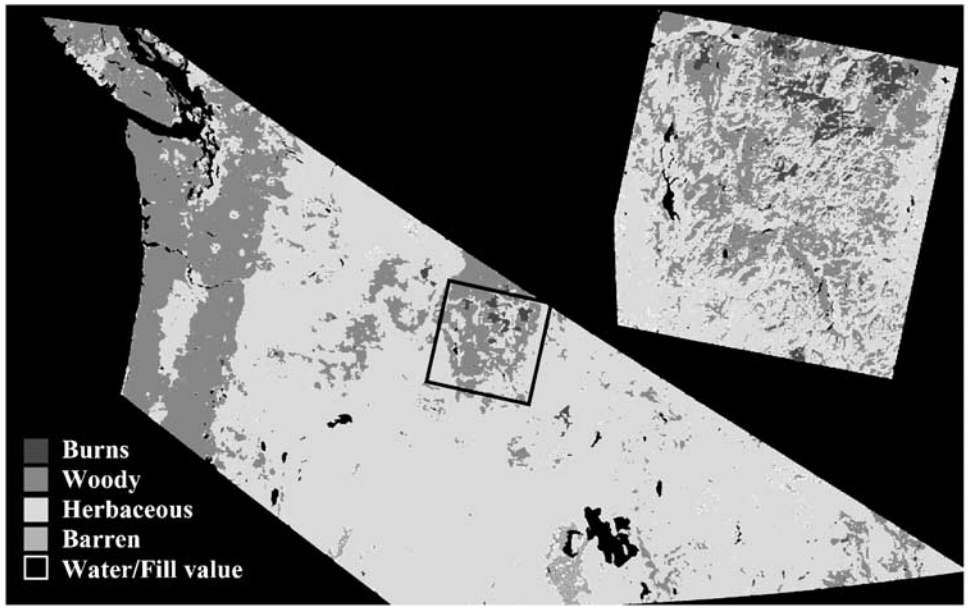

Figure 4. The ARTMAP discrete classification of the MODIS and the ETM+ surface reflectance data. See color version of this figure at back of this issue.

error but a high commission error. The burn class has high commission and omission errors (0.98/0.67). Several factors are responsible for the above discrepancy. According to the product quality control documentation (site 4 in Table 1), the MODIS fire product has low accuracy prior to November 2000 because of the poor quality of mid IR data, which may contribute both to commission and omission errors. Also, commission errors are due to the fact that the reference data set does not cover all the fire events resulted in the detected burns. The MODIS fire product sample only 24 days (from 20 August to 5 September of year 2000), while, according to the ground sources, the major fires in Idaho and Montana took place during July–August in year 2000. Another reason for commission errors is that the MODIS overpass temporal frequency is not sufficient to follow the evolution of all active fires. Therefore a commission error cannot serve as a reliable indicator of uncertainties in a burn map. An omission error (a fire was detected, but no burns were detected) is the only reasonable indicator of the uncertainties of fire and burn products.

[26] To assess the uncertainties in omission errors, we performed intercomparison of the detected burns with independent reference data sets (fires from MODIS and ATSR). The comparison was performed on the basis of the rough set methodology (Appendix A), which quantifies uncertainties in terms of set lower and upper approximations. Table 5 summarizes omission errors when comparing the ARTMAP detected burns with the ATSR algorithm 1 and 2 fires, the MODIS fire product and the union of the above data sets. For example, omission errors can vary from 0.67 to 0.60 in the case when the MODIS fire product is used as a reference. The similar range of the variations of omission errors were found when the ATSR fire products were used as a reference. However, if the MODIS and the ATSR fire products are combined (union of two data sets), the omission error is significantly lower. For instance, the range of variation of omission errors for the combined MODIS and ATSR algorithm 1 fire products is [0.43, 0.38]. This suggests that different fire products sample partially overlapping fire events, and none of the products has a complete record of all fires. The incompleteness of the fire record as well as the uncertainties of the fire products set a limit to the accuracy of the performed comparison with the detected burns.

3.3. Evaluation of the Impact of Land Cover Mixture on Burn Detection

[27] The MODIS 500-m surface reflectance product provides a coarse-resolution data source for burns mapping. At this scale, burns are highly mixed with other land cover

Table 4. Error Matrix for the MODIS Discrete Classification and the Reference Data Set[a]

	Reference					
	Burns	Woody	Herbaceous	Barren	Grades	Commission
ARTMAP						
Burns	**3,416**	52,276	87,776	359	143,827	0.98
Woody	2,999	**1,645,872**	657,104	255	2,306,230	0.29
Herbaceous	3,672	479983	**6,201,521**	15,816	6,700,992	0.17
Barren	42	10531	145,251	**37,783**	193,607	0.80
Grades	10,129	2,188,662	7,091,652	54,213		
Omission	0.67	0.25	0.23	0.30		

[a]MODIS land cover overlaid with the MODIS fire product. Sample total is 9,344,656. Overall accuracy is 84.5%. Boldface (diagonal values) indicates agreement.

Table 5. Lower and Upper Approximations of Omission Errors for the Burn Class, Assessed With the Different Reference Fire Products MOD14A2 and ATSR-2 Global Fire Atlas

	Lower Approximation	Upper Approximation
MOD14A2	0.67	0.60
ATSR algorithm 1	0.61	0.54
ATSR algorithm 2	0.62	0.56
ATSR algorithm 1 ∩ MOD14A2	0.43	0.38
ATSR algorithm 2 ∩ MOD14A2	0.45	0.40

types. This mixture introduces substantial uncertainties in burn detection from the discrete classification. High-resolution satellite data, such as 30-m ETM+ surface reflectances, provide required information to assess the impact of land cover mixture on burn detection.

[28] We performed the ARTMAP discrete classification of the ETM+ scene with training data described in the previous section (see Figure 3b). The resulting classification image was aggregated from a 30-m to 500-m scale (each coarse-resolution pixel contains $17 \times 17 = 289$ subpixels). For each aggregated ETM+ pixel, we calculated the proportion of pixels with a given class to the total amount of subpixels in each aggregated pixel. We refer to this quantity as "purity" below. Figure 5 demonstrates the spatial distribution of purity for burns (Figure 5a), woody vegetation (Figure 5b) and herbaceous vegetation (Figure 5c). Note the high purity of burns for several clusters at the top of Figure 5a, which corresponds to the clusters of burns in Figure 4. Woody vegetation has high purity for the majority of the pixels, except for the low values over the areas of burns and over few patches with herbaceous vegetation. Herbaceous vegetation has uniformly low purity over the entire scene.

[29] A subset of the MODIS classification over the spatial extent of the ETM+ scene (Figure 4) was extracted for comparison purposes. Figure 6 compares the spatial distribution of burns detected from the MODIS surface reflectance data (Figure 6a) and the ETM+ aggregated data

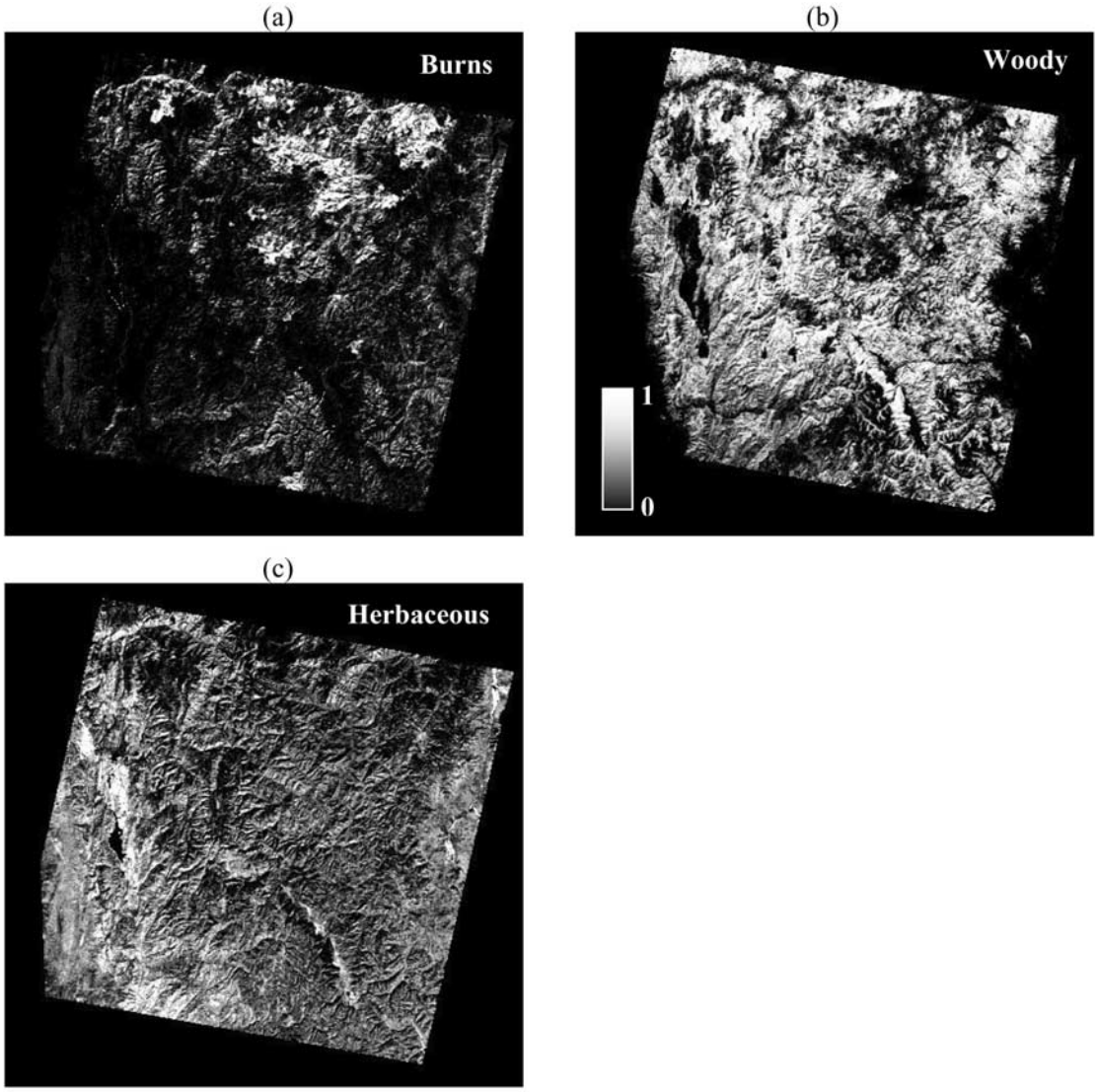

Figure 5. Subpixel percentages of land cover mixtures at 500-m scale derived from the aggregation of the 30-m ETM+ discrete classification. Three predominant classes in the scene are shown: (a) burns, (b) woody vegetation, and (c) herbaceous vegetation.

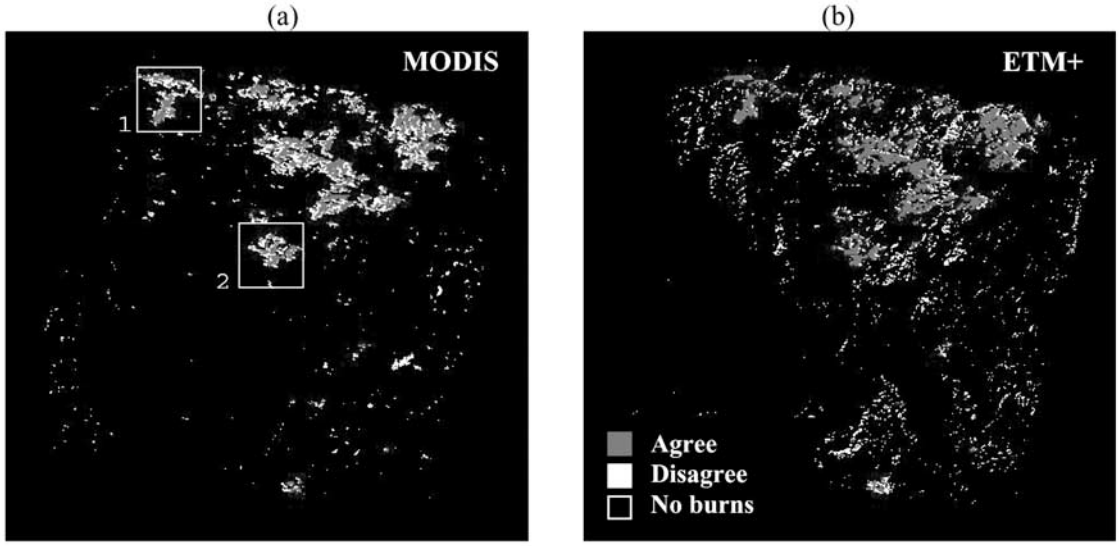

Figure 6. Comparison of spatial distributions of burns identified by the discrete classification of the (a) MODIS and (b) ETM+ surface reflectance data. The ETM+ classification was aggregated to 500-m spatial resolution, and pixels were assigned to burn class if burn purity is higher than 50%. The grey pixels indicate areas where both classifications agree, while the white pixels mark areas where only one data set identifies burns. Rectangles with white boundaries (marked "1" and "2") show the location of two patches selected for further comparison.

(Figure 6b). The purity threshold of 50% separates burn and no-burn pixels at the ETM+ aggregated classification. The pixels where the MODIS and the ETM+ burn classifications agree are marked in grey, while the pixels where only a single data set indicates burns are marked in white. The spatial distribution of pixels where both classifications agree covers uniformly major clusters of burns. In contrast, disagreement can be noted for scattered pixels with neighborhood sparsely populated by burns.

[30] Figure 7 summarizes the results of the numerical analysis of agreement/disagreement between the detected burns in the MODIS and the ETM+ classifications as function of purity of the aggregated ETM+ data. First, consider results for the ETM+ classification. Figure 7a shows the distribution of the amount of pixels with burns as function of purity. Note that as purity increases, the amount of burned pixels decreases with the rate exceeding the exponential law. This result indicates the overall dominance of pixels with mixture in the scene. Figure 7c compares the amount of pixels, for which the ETM+ aggregated and the MODIS classifications agree or disagree. One can note the large amount of pixels with burns in the ETM+ image which are not classified as burns in the MODIS image at the low threshold on purity (<20%). The reason is as follows. At the low threshold on purity, signal from small islands of burns is weak relative to the signal from other land cover classes in the pixel, and therefore it cannot be accurately captured by the MODIS discrete classification (high rate of omission).

[31] Next, consider results for MODIS burns. The distribution of the amount of MODIS pixels with burns as function of purity on the ETM+ aggregated classification is shown in Figure 7b. The distribution is flat, except for the peak at low purity. This peak corresponds to disagreement between the MODIS and the ETM+ classifications because of the uncertainties in the input and training data sets and accounts for a minor portion of MODIS burned pixels (6%). Flat distribution of detected moderate- and high-purity burn pixels suggests that MODIS discrete classification capture burns if signal comes from predominant burn class. Also, the ratio of MODIS to ETM+ histograms is an increasing function of purity (see Figure 7b) which indicates that pixels with high purity of burns have less chance to be misidentified by the MODIS discrete classification. The amount of MODIS pixels with burns, where the ETM+ data indicate no burns, nearly linearly increases as purity increases, as can be seen in Figure 7c. The increase of disagreement is due to the following. The set of ETM+ pixels with burns can only decrease as purity increases: ETM+ pixels marked as burns at the low-purity threshold will be marked as nonburns for a high-purity threshold. The set of burned MODIS pixels does not change with the variation of purity. Therefore as purity increases, some ETM+ pixels with burns, corresponding to the MODIS pixels with burns, will be converted to nonburns, which results in an increase of disagreement.

[32] The impact of land cover mixture on burn detection can be further illustrated by comparing spatial subsets of the MODIS and the ETM+ classifications at original resolutions (500 m and 30 m, respectively) for several major clusters of burns, as shown in Figure 8. We selected two subsets, referred to as "patch 1" and "patch 2," as shown in Figure 6a. In general, both the MODIS and the ETM+ classifications show similar spatial patterns of burns for large homogeneous clusters of burns. The mountain ranges separate burned and nonburned areas, which is well captured by fine and coarse-resolution imagery. Inspection of the details of burned patches indicates large heterogeneity, mixture of land cover types, detected with the ETM+ classification and smoothed-out with the MODIS classification. For instance, areas at the top of the image for "patch 1" along the mountain ranges are marked as continuous burns according

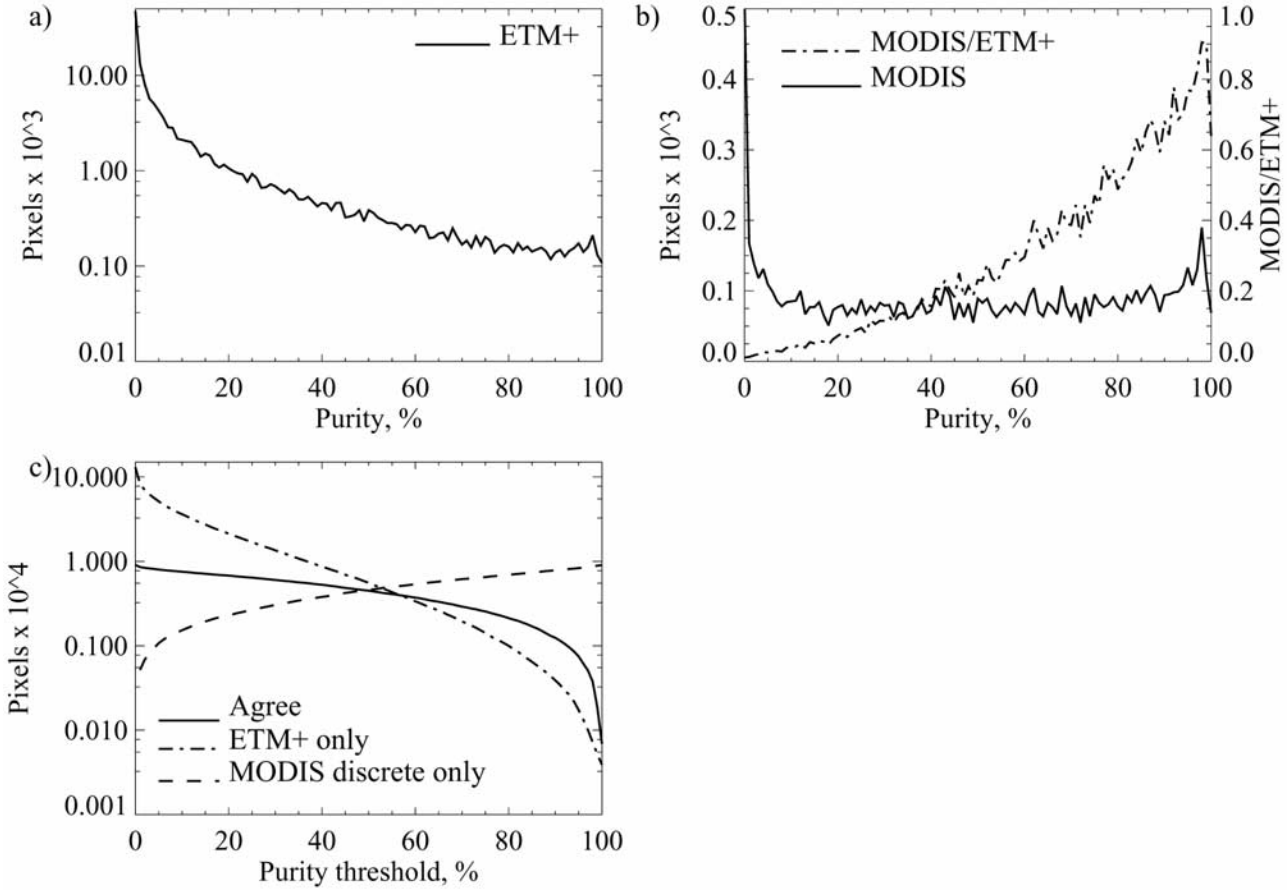

Figure 7. Analysis of the consistency of burn mapping from the MODIS discrete and the ETM+ aggregated classifications. (a) Distribution of the amount of burned pixels in the ETM+ aggregated classification as a function of the ETM+ pixel purity. (b) Distribution of the amount of pixels with burns in the MODIS discrete classification as a function of the ETM+ pixel purity. Also shown is the ratio of MODIS to ETM+ distributions. (c) Distribution of the amount of pixels where both MODIS and ETM+ classifications simultaneously detect burns as a function of the threshold on the ETM+ pixel purity. Also shown is the distribution of the amount of pixels where only the MODIS or only the ETM+ classification detects burns.

to the MODIS classification, while the ETM+ classification demonstrates significant land cover heterogeneity in these areas. Multiple cases of omissions/commissions errors in the MODIS classification can be found at "patch 2," when referencing high-resolution imagery.

[33] In summary, burn mapping from discrete classification of the coarse-resolution imagery is generally consistent with burn mapping from aggregated classification of fine-resolution imagery only for large homogeneous clusters of burns. However, for a very typical case of mixture of burns with other land cover types, commission/omission errors dominate burn detection from coarse-resolution imagery. This observation highlights the need for continuous classification of burns as an alternative approach that is sensitive to land cover mixtures. This approach will be discussed next.

4. Burn Detection From the Continuous Classification of MODIS Surface Reflectance Data

4.1. Training Strategy

[34] Training of the ARTMAP mixture model requires sampling of variability in the relative proportion (percentages) of four land cover classes (burns, woody, herbaceous and bare) over the observed range of surface reflectances in the MODIS image. In this research we referenced mixture percentages at 500-m scale, derived from the ETM+ aggregated classification (see section 3). This data set is a surrogate for actual field measurements. However, at 30-m ETM+ scale the mixture of land cover classes is low and pixels can be assumed pure; the aggregation of 30-m pixels to 500-m scale can provide reasonable quality estimation of land cover mixtures. Additionally, a field sampling of percentages of land cover classes at 500-m scale is a laborious task, which has limitation on the accuracy and coverage of spatial variability.

[35] Sampling of training data for the continuous classification requires collection of more information than in the case of the discrete classification (the location of class purity percentages versus the location of class in spectral space). What is the optimal sampling strategy for training the ARTMAP mixture model? The simplest approach is to select pixels randomly from an image. Given a sufficiently large data set, one can establish a relationship between surface reflectances (RED and NIR) and mixture percen-

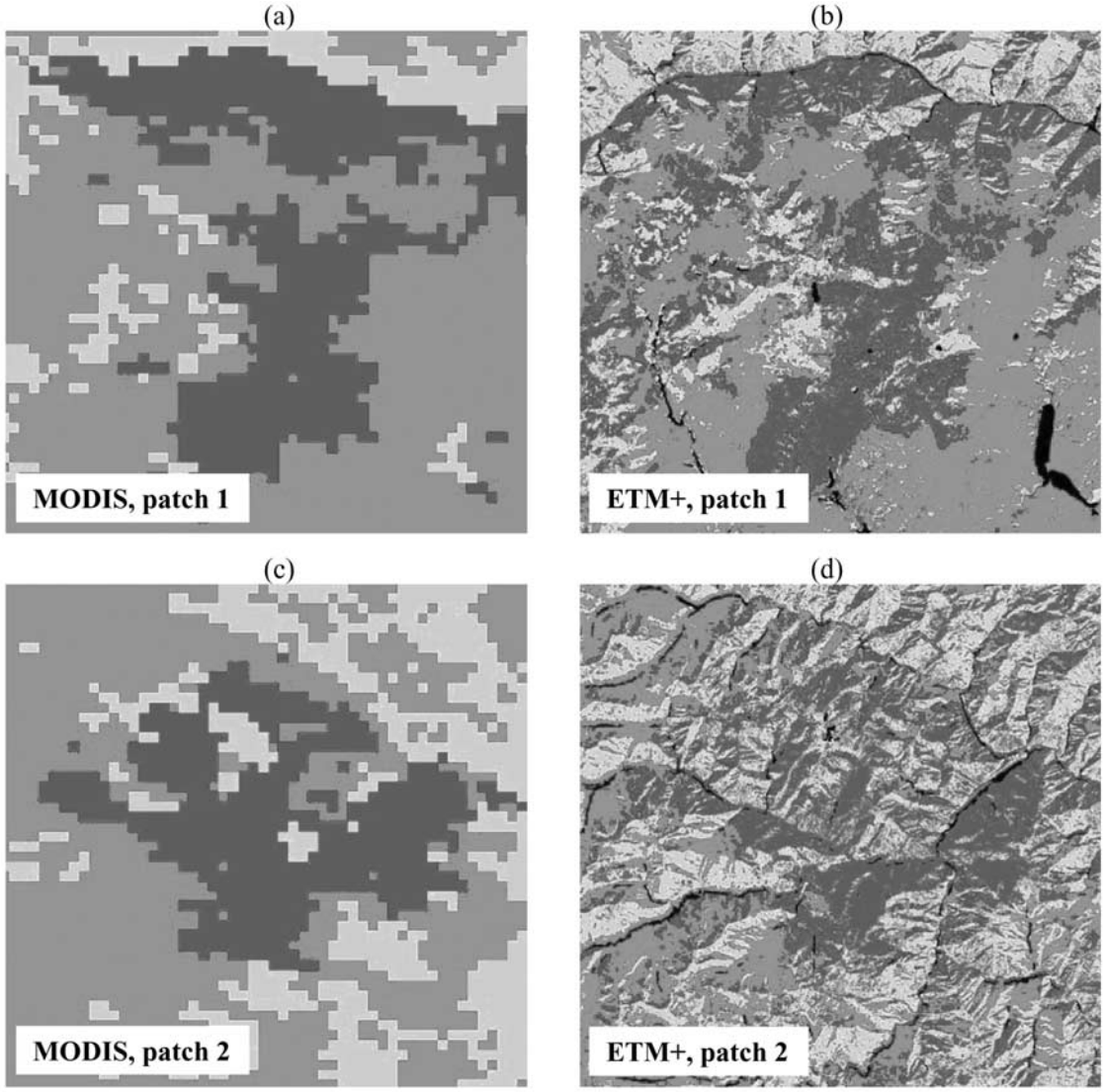

Figure 8. Comparison of spatial distribution of burns at 500-m (the MODIS discrete classification) and 30-m scale (the ETM+ discrete classification) for (a and b) "patch 1" and (c and d) "patch 2."

tages. However, while unconstrained random sampling accumulates required statistics, it will also accumulate outliers. Even a small number of outliers can introduce significant confusion in the ARTMAP decision space. Therefore, in selection of training data for the continuous classification we used the same paradigm of majority rule as we did for the discrete classification. Specifically, the procedure of sampling training data is as follows. RED-NIR spectral space was divided into a set of 100 × 100 equal bins (ΔRED = ΔNIR = 0.01 for each bin). Given the value of RED and NIR reflectances for each bin, the corresponding mean and standard deviation of percentages of each land cover class were calculated, referencing the MODIS surface reflectances and land cover percentages from the ETM+ aggregated classification. This procedure establishes functional dependence of land cover mixtures on surface reflectances in a statistical sense. Next, training data set was constructed from about 3000 pixels selected randomly over the extent of ETM+ image such that range of variations of class mixture percentages for a given value of surface reflectances was within one standard deviation from the mean value, evaluated in the previous step.

[36] The decision space generated by ARTMAP mixture model based on the above training data set is shown in Figure 9. Note the similarity between the location of spectral signatures of high-purity land cover classes for continuous classification and the corresponding signatures for the discrete classification (see Figure 3a). The probability of class membership for the continuous classification decreases with respect to the distance from its most probable location in spectral space. Land cover class purity changes with the location in spectral space in a nonlinear fashion which was possible to capture with the ARTMAP mixture model but cannot be achieved with the linear mixture model. Note also, that classes have a significant area of overlapping at moderate purity, corresponding to land cover mixtures.

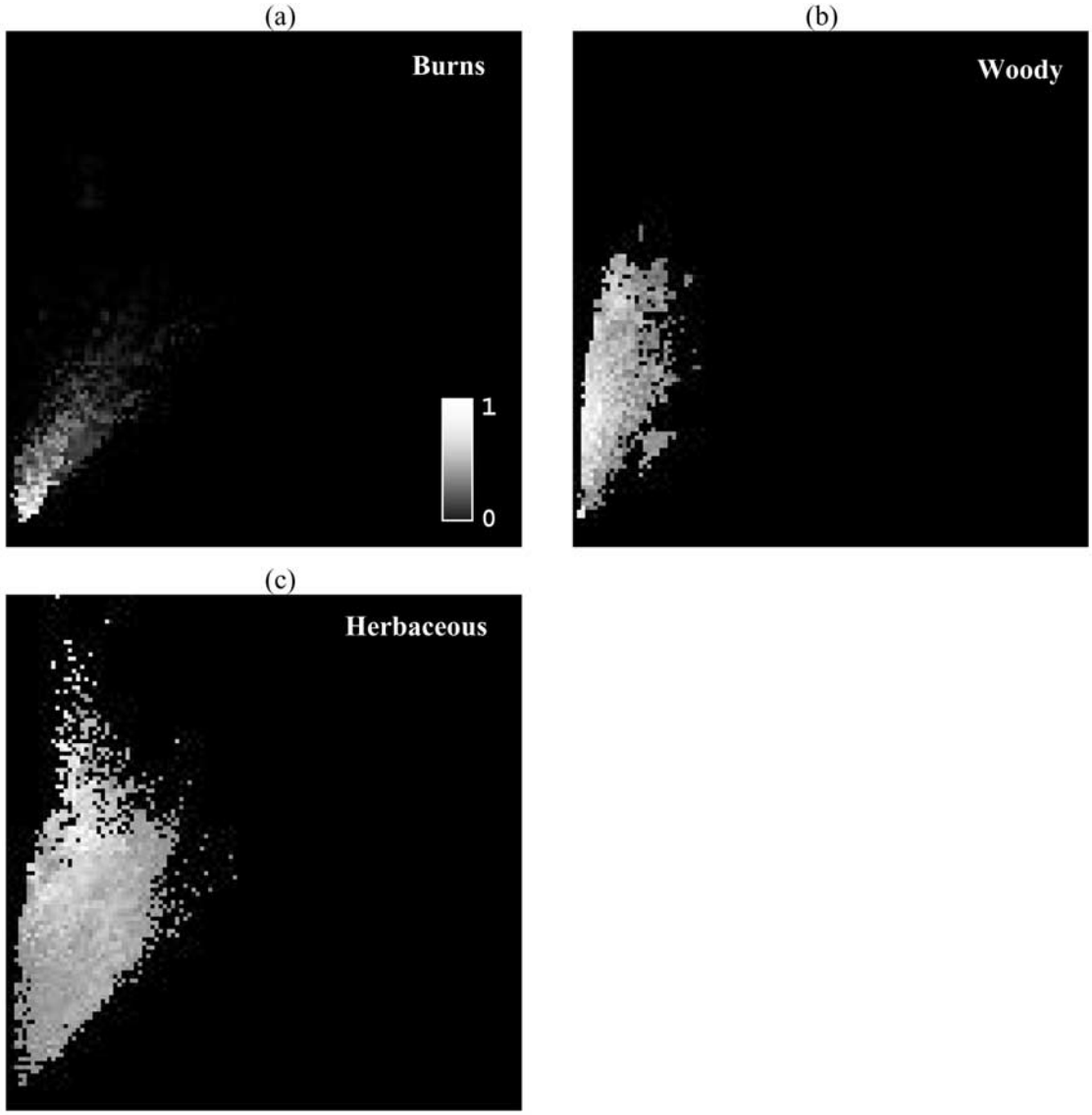

Figure 9. ARTMAP decision space for the MODIS continuous classification. Distribution predicted by ARTMAP of subpixel percentages of (a) burns, (b) woody vegetation, (c) and herbaceous vegetation in the RED-NIR spectral space, when input vectors are restricted to the observed values of surface reflectances data.

4.2. Analysis of Continuous Classification

[37] Figure 10 presents the continuous classification of MODIS surface reflectances data for burns, woody and herbaceous classes. Compare the spatial features of this classification with the corresponding features of the MODIS discrete (Figure 6a) and the ETM+ aggregated (Figure 6b) classifications. The MODIS continuous classification captures all the major clusters of burns detected in the MODIS discrete and the ETM+ aggregated classifications. In addition, it enhances the MODIS discrete classification in terms of capturing burns with a lower probability at the boundaries or inside of large clusters of burns. Burn clusters detected by continuous classification more closely follow the boundaries of the mountains ranges and the shape of the landscape. The MODIS continuous classification identifies scattered burn signals at low probability in the bottom of the image, which was not achieved by the MODIS discrete classification. The detection of scattered burns at low probability using the continuous classification helps resolve the problem of burns underestimation, identified in the previous section. Note also, that the bottom left portion of the burn image has mostly a zero probability of burns, because of a high purity of identified woody and herbaceous vegetation classes (see Figure 5). However, the comparison of the ETM+ aggregated classification and the MODIS continuous classifications suggests that the latter smoothes the sharp details of the former. This is due to the fact that MODIS coarse-resolution surface reflectances provide lower information content than high-resolution ETM+ data, and class unmixturing is only an approximation to mixture estimation from high-resolution satellite data. Visual comparison of the input surface reflectances was performed for several subsets of MODIS and ETM+ data and confirms the facts that MODIS surface reflectance data sometimes do not

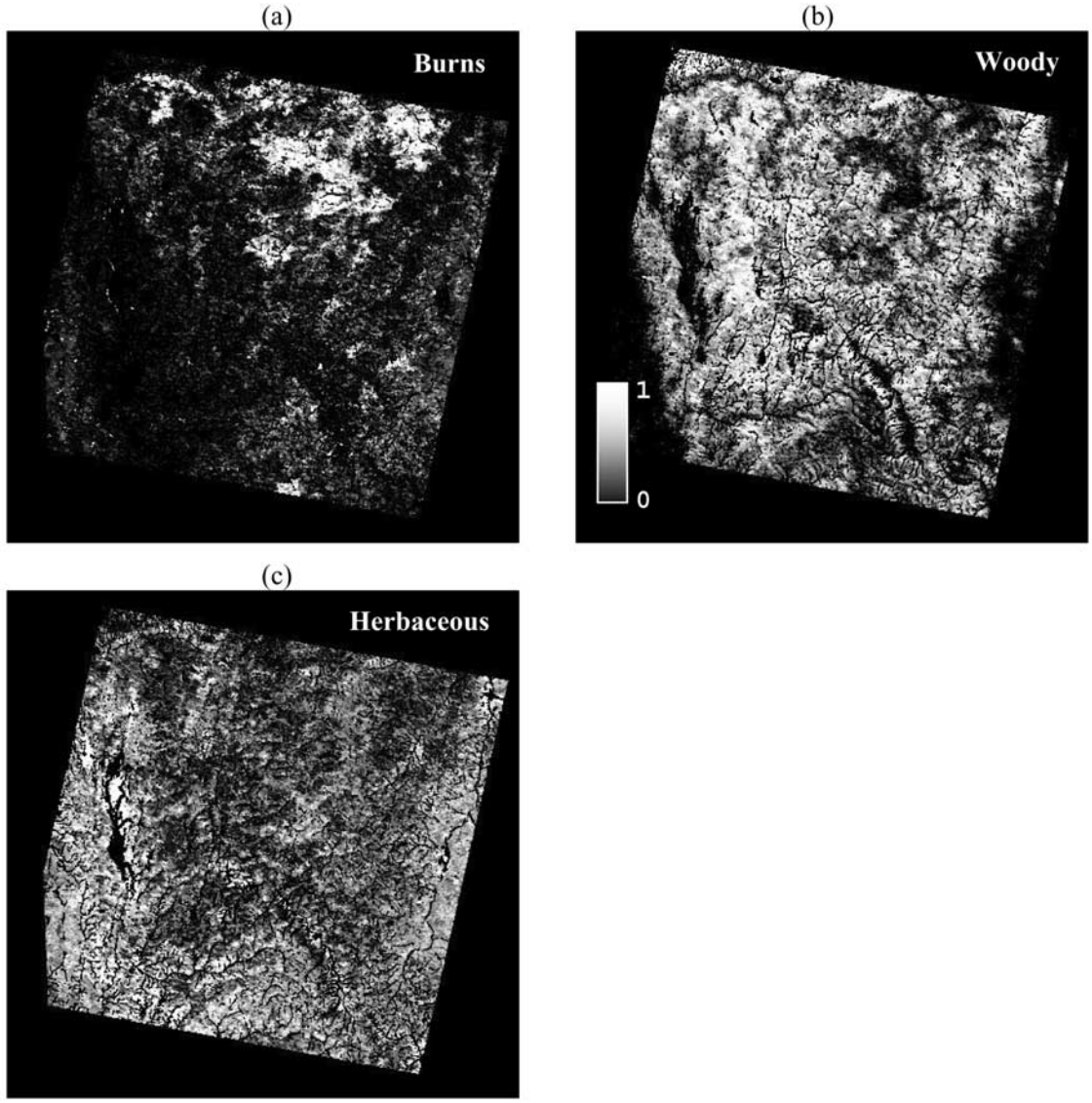

Figure 10. Subpixel percentages of land cover mixtures from continuous classification of MODIS 500-m surface reflectances. Three predominant classes in the scene are shown: (a) burns, (b) woody vegetation, and (c) herbaceous vegetation.

provide sharp distinction of landscape features available from aggregated ETM+ data.

[38] We applied the numerical analysis described in section 3 to compare the MODIS continuous and discrete and the ETM+ aggregated classifications. The results are presented in Figure 11. The histogram of the MODIS continuous classification of burns as function of purity closely follows the ETM+ plot, as shown in Figure 11a. This means that a relative proportion of burn purities was well captured by the MODIS continuous classification. Variations are due to the limited sampling and the smoothing effect of MODIS surface reflectance data, mentioned above. Figure 11b compares the amount of pixels where MODIS continuous and the ETM+ aggregated classifications agree and disagree. Note that the agreement rate is higher than the disagreement rate in case of the MODIS continuous classification for a wide range of purity thresholds. The disagreement with ETM+ data is due to the scattered burns at the lower portion of the ETM+ image, which were not captured in full by the MODIS continuous classification because of the reasons mentioned above. Figure 11c compares the MODIS continuous and discrete classifications. Note the sharp decrease in disagreement of the MODIS continuous classification at purity >70%. This indicates that the MODIS continuous classification is more conservative than the MODIS discrete classification: It detects all high-purity burns identified by the discrete classification and sets the rest to lower purity. This addresses the issue of burn area overestimation, as discussed in the previous section. Additional indication of decreasing commission/omission errors can be found in Tables 6 and 7, which compare the ETM+ aggregated classification with the MODIS discrete and the continuous classifications using fuzzy error matrix concepts [*Zadeh*, 1965; *Binaghi et al.*,

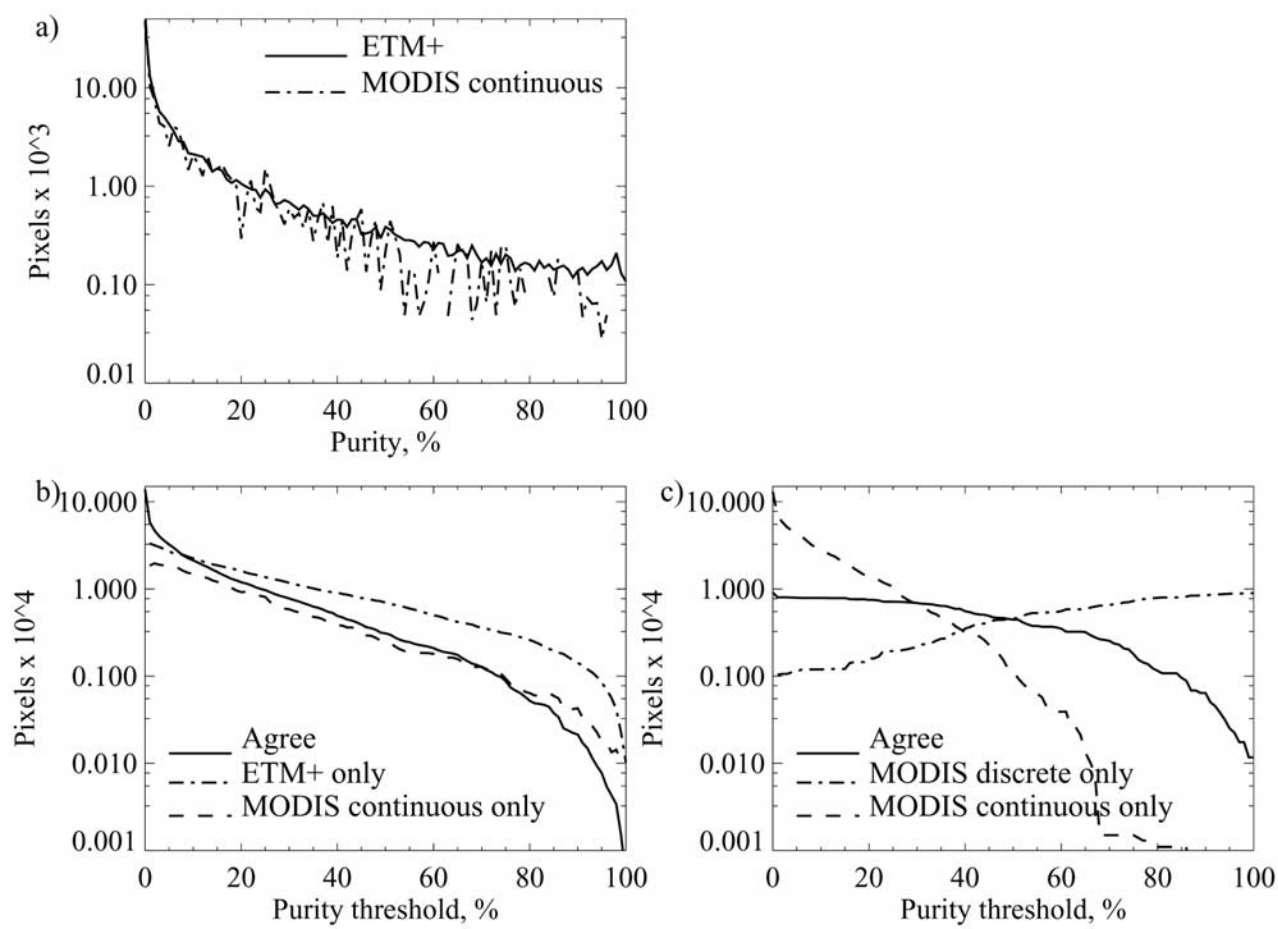

Figure 11. Analysis of the consistency of burn mapping from the MODIS continuous/discrete and the ETM+ aggregated classifications. (a) Distribution of the amount of pixels with burns in the MODIS continuous and the ETM+ aggregated classifications as function of pixel purity. (b) Distribution of the amount of pixels where both the MODIS continuous and the ETM+ aggregated classifications simultaneously detect burns as function of the threshold on the pixel purity. Also shown is the distribution of the amount of pixels where only the MODIS continuous or only the ETM+ aggregated classification detects burns. (c) Same as Figure 11b but analysis performed for the MODIS continuous and discrete classifications.

1999]. Omission errors for burns decreased from 0.74 to 0.56 and corresponding commission errors decreased from 0.52 to 0.40. Commission/omission errors for the other classes also improved in various degrees, especially for the barren class, which was significantly overestimated by the discrete classification. The overall agreement of the ETM+ classification with the MODIS discrete classification is 49.5%, while the agreement of ETM+ classification with the MODIS continuous classification is 55.3%.

[39] Concluding this section, we want to emphasize the difference in the utilization of fine and course-resolution data in the proposed technology. ETM+ high-resolution data

Table 6. Fuzzy Error Matrix for the MODIS Discrete and the ETM+ Aggregated Classifications[a]

	ETM+					
	Burns	Woody	Herbaceous	Barren	Grades	Commission
MODIS						
Burns	**4,396.06**	0.0	0.0	0.0	9058	0.52
Woody	0.0	**44,410.8**	0.0	0.0	75,697	0.41
Herbaceous	0.0	0.0	**19,693.9**	0.0	53,519	0.63
Barren	0.0	0.0	0.0	**2.76**	4	0.31
Grades	16,642.6	58,012.8	40,995.8	20,313.6		
Omission	0.74	0.23	0.52	1.0		

[a]Sample total is 138,278. Overall accuracy is 49.5%.

Table 7. Fuzzy Error Matrix for the MODIS Continuous and the ETM+ Aggregated Classifications[a]

	ETM+					
	Burns	Woody	Herbaceous	Barren	Grades	Commission
MODIS						
Burns	**7,399.97**	6,377.05	6,713.19	4,666.48	12,356	0.40
Woody	7,899.02	**37,306.7**	20,728.8	7,315.75	51,583.1	0.28
Herbaceous	7,630.12	17,721.2	**22,460.1**	12,319.1	31,682.5	0.29
Barren	4,556.87	5,046.32	10,339.7	**9,356.06**	13,582.7	0.31
Grades	16,642.6	58,012.8	40,995.8	20,313.6		
Omission	0.56	0.36	0.45	0.54		

[a]Sample total is 138,278. Overall accuracy is 55.5%.

are required for training purposes only to establish the ARTMAP mixture model. Training also requires one scene of coarse-resolution data to relate the ETM+ derived land cover mixture percentages with signatures of course-resolution surface reflectance data. The only restriction on training data is that fine and course-resolution images used for training should be collected within the time interval when changes in burn area are minimal between the data sources. Once trained, the ARTMAP mixture algorithm reference only coarse-resolution surface reflectances data to perform burn detection for a given sequence (in terms of time and space) of MODIS scenes.

5. Conclusions

[40] This paper presented a neural network approach for the detection of burns from coarse-resolution satellite imagery using two methods: the discrete and the continuous classifications. The continuous approach to burn mapping helps to resolve the problem of overestimation/underestimation of burn areas frequently encountered with conventional discrete classification schemes. The training of the ARTMAP mixture algorithm was based on high-resolution ETM+ data. Once trained, the ARTMAP mixture algorithm references only coarse-resolution surface reflectances data to perform burn detection for a given sequence (in terms of time and space) of MODIS scenes. Therefore the proposed technology provides benefits of accurate, frequent and low-cost burn monitoring from coarse-resolution data at regional scale.

[41] There are several sources of uncertainties associated with burn mapping by the proposed method. The first source is related to training of the ARTMAP classifier. In general, the burn class has distinct spectral signatures of low RED and NIR reflectances in contrast to spectral signatures of vegetation. However, confusion between burns and dark bare soil is possible. Selection of signatures of nonburn classes can be performed relatively easily by referencing existing land cover products, but training for burns is more involved, because of the low availability of reliable references (ground surveys or satellite fire products). The second source of uncertainties is an impact of atmosphere on the quality of the input surface reflectance data. For instance, clouds can substantially obscure burned areas in the image selected for classification.

[42] Finally, the presented research should be considered as the introduction to the topic of continuous burn mapping and address basic implementation issues. Extensive testing of the algorithm at various environmental conditions (i.e., burns in woody versus herbaceous vegetation at different climatic zones and seasons) is required in the future to fully quantify its performance and assess the uncertainties of burn retrievals.

Appendix A: Rough Sets

[43] The rough set was initially introduced as a mathematical tool in support of automated reasoning. Recent applications [*Bjorvand*, 1997] include object-oriented data-mining and knowledge discovery applications. Rough sets are useful in representing uncertainty related to spatial data in both remote sensing and Geographic Information Systems [*Pawlak*, 1982].

[44] A rough set is a pair $(\underline{X}, \overline{X})$ of standard sets, the lower approximation and the upper approximation of the set X, such that $\underline{X} \subseteq \overline{X}$. The interpretation of lower and upper boundaries is as follows: (1) If we have item A, $A \subset \underline{X}$, it means that A definitely belongs to set X; (2) if we have A, $A \subset \overline{X} - \underline{X}$, it means we are not sure if element A belongs to set X; (3) if we have A, $A \not\subset \overline{X}$, it means that A definitely does not belong to set X. Standard sets, or crisp sets, are just special case of rough sets, when $\underline{X} = \overline{X}$. The basic set operations can be extended to rough sets as follows: union, $(\underline{X}, \overline{X}) \cup (\underline{Y}, \overline{Y}) = (\underline{X} \cup \underline{Y}, \overline{X} \cup \overline{Y})$; intersection, $(\underline{X}, \overline{X}) \cap (\underline{Y}, \overline{Y}) = (\underline{X} \cap \underline{Y}, \overline{X} \cap \overline{Y})$; and negation, $(\underline{X}, \overline{X})^* = (-\overline{X}, -\overline{X})$. When comparing a standard set with a rough set, one needs to extend the definition of confusion matrix. Let X consists of rough classes $(\underline{X}_k, \overline{X}_k)$, $k \in K$ and Y consist of crisp classes Y_l, $l \in L$. The extended confusion matrix will be of size $2K \times L$, and its elements $x_{i,k}$ are defined as follows. $x_{i,k} = \underline{X}_k \cap Y_i$, if k is odd and $x_{i,k} = \overline{X}_k \cap Y_i$, if k is even. In the context of the presented research, we are using rough sets to evaluate uncertainty of the ARTMAP classification of MODIS surface reflectances when comparing to the two fire products (from MODIS and ATSR). The ARTMAP classification results can be treated as rough sets, when considering the primary classification results as lower boundary, while the secondary image combined with the primary image provides the upper approximation. The MODIS and the ATSR fire products are treated as crisp sets.

[45] **Acknowledgments.** This research was conducted as part of NASA's Intelligent Data Understanding (IDU) program. We gratefully acknowledge financial support through grant NCC 2-1233. The authors thank W. Liu for the help with the ARTMAP code. We also thank anonymous reviewers for their thoughtful comments.

References

Abuelgasim, A., W. Ross, S. Gopal, and C. Woodcock (1999), Change detection using adaptive fuzzy neural networks, Environmental damage assessment after the Gulf War, *Remote Sens. Environ.*, *70*(2), 208–223.

Arino, O., M. Simon, I. Piccolini, and J. M. Rosaz (2001), The ERS-2 ATSR-2 World Fire Atlas and the ERS-2 ATSR-2 World Burnt Surface Atlas projects, paper presented at 8th ISPRS conference on Physical Measurement and Signatures in Remote Sensing, Int. Soc. for Photogramm. and Remote Sens., Aussois, France, 8–12 Jan.

Binaghi, E., P. A. Brivio, P. Ghezzi, and A. Rampini (1999), A fuzzy set-based accuracy assessment of soft classification, *Pattern Recognit. Lett.*, *20*, 935–948.

Bjorvand, A. T. (1997), Rough enough—A system supporting the rough sets approach, *Ser. Publ. C*, vol. 49, pp. 99–110, Dep. of Comput Sci., Univ. of Helsinki, Helsinki.

Brivio, P. A., M. Maggi, E. Binaghi, and I. Gallo (2003), Mapping burned surfaces in sub-Saharan Africa based on multi-temporal neural classification, *Int. J. Remote Sens.*, *24*, 4003–4018.

Carpenter, G. (1997), Distributed learning, recognition, and prediction by ART and ARTMAP neural networks, *Neural Networks*, *10*, 1473–1494.

Carpenter, G., S. Grossberg, N. Martens, J. Reynolds, and D. Rosen (1992), Fuzzy ARTMAP: A neural network architecture for incremental supervised learning of analog multidimensional maps, *IEEE Trans. Neural Networks*, *3*, 698–713.

Carpenter, G., S. Gopal, S. Macomber, S. Martens, C. Woodcock, and J. Franklin (1999a), A neural network method for efficient vegetation mapping, *Remote Sens. Environ.*, *70*, 326–338.

Carpenter, G., S. Gopal, S. Macomber, S. Martens, and C. Woodcock (1999b), A neural network method for mixture estimation for vegetation mapping, *Remote Sens. Environ.*, *70*, 138–152.

DeFries, R. S., J. R. G. Townshend, and M. C. Hansen (1999), Continuous fields of vegetation characteristics at the global scale at 1-km resolution, *J. Geophys. Res.*, *104*(D14), 16,911–16,923.

Eva, H., and E. F. Lambin (1998), Burnt area mapping in central Africa using ATSR data, *Int. J. Remote Sens.*, *19*, 3473–3497.

Fraser, R. H., Z. Li, and J. Cihlar (2000), Hotspot and NDVI differencing synergy (HANDS): A new technique for burned area mapping over boreal forest, *Remote Sens. Environ.*, *74*, 362–376.

Friedl, M. A., D. K. McIver, J. C. F. Hodges, X. Y. Zhang, D. Muchoney, A. H. Strahler, C. E. Woodcock, S. Gopal, A. Schneider, and A. Cooper (2002), Global land cover mapping from MODIS: Algorithms and early results, *Remote Sens. Environ.*, *83*, 287–302.

Gopal, S., C. Woodcock, and A. Strahler (1999), Fuzzy neural network classification of global land cover from 1 degree AVHRR data set, *Remote Sens. Environ.*, *67*, 230–243.

Grossberg, S. (1976), Adaptive pattern classification and universal recoding, I Parallel development and coding of neural feature detectors, *Biol. Cybern.*, *23*, 121–134.

Hansen, M. C., R. S. DeFries, J. R. G. Townshend, R. Sohlberg, C. Dimiceli, and M. Carroll (2002), Towards an operational MODIS continuous field of percent tree cover algorithm: Examples using AVHRR and MODIS data, *Remote Sens. Environ.*, *83*, 303–319.

Justice, C. O., L. Giglio, S. Korontzi, J. Owens, J. T. Morisette, D. Roy, J. Descloitres, S. Alleaume, F. Petitcolin, and Y. Kaufman (2002), The MODIS fire products, *Remote Sens. Environ.*, *83*, 244–262.

Kasischke, E. S., and N. H. F. French (1995), Locating and estimating the areal extent of wildfires in Alaskan boreal forests using multiple-season AVHRR NDVI composite data, *Remote Sens. Environ.*, *51*, 263–275.

Levine, J. S., W. R. Cofer III, D. R. Cahoon Jr., and E. L. Winstead (1995), Biomass burning: A driver for global change, *Environ. Sci. Technol.*, *29*, 120–125.

McDonald, A. J., F. M. Gemmell, and P. E. Lewis (1998), Investigation of the utility of spectral vegetation indices for determining information on coniferous forests, *Remote Sens. Environ.*, *66*, 250–272.

McIver, D. K., and M. A. Friedl (2002), Using prior probabilities in decision-tree classification of remotely sensed data, *Remote Sens. Environ.*, *81*, 253–261.

Pawlak, Z. (1982), Rough sets, *Int. J. Comput. Inf. Sci.*, *11*, 341–356.

Roy, D. P., P. E. Lewis, and C. O. Justice (2002), Burned area mapping using multi-temporal moderate spatial resolution data—A bi-directional reflectance model-based expectation approach, *Remote Sens. Environ.*, *83*, 263–286.

Scholes, R. J. (1995), Greenhouse gas emissions from vegetation fires in southern Africa, *Environ. Monit. Assess.*, *38*, 169–179.

Schowengerdt, R. A. (1996), On the estimation of spatial-spectral mixing with classifier likelihood functions, *Pattern Recognit. Lett.*, *17*, 1379–1387.

Sellers, P. J., et al. (1995), The Boreal Ecosystem-Atmosphere Study (BOREAS): An overview and early results from 1994 field year, *Bull. Am. Meteorol. Soc.*, *76*, 1549–1577.

Vermote, E. F., N. Z. El Saleous, C. O. Justice, Y. J. Kaufman, J. Privette, L. C. Remer, and D. Tanre (1997), Atmospheric correction of visible to middle infrared EOS-MODIS data over land surface, background, operational algorithm and validation, *J. Geophys. Res.*, *102*(D14), 17,131–17,141.

Vermote, E. F., N. Z. El Saleous, and C. O. Justice (2002), Atmospheric correction of MODIS data in the visible to middle infrared: First results, *Remote Sens. Environ.*, *83*, 97–111.

Zadeh, L. (1965), Fuzzy sets, *Inf. Control*, *8*, 338–353.

Zhan, X., C. Huang, J. R. G. Townshend, R. DeFries, M. Hansen, C. DiMiceli, R. Sohlberg, J. Hewson-Scardelletti, and A. Tompkins (1998), Land cover change detection with change vector in the red and near-infrared reflectance space, in *Proceedings of the 1998 IEEE International Geoscience and Remote Sensing Symposium IGARSS'98*, *Seattle*, *Washington*, *6–10 July 1998*, vol. II, pp. 859–861, IEEE Press, Piscataway, N. J.

Zhan, X., R. Sohlberg, J. R. G. Townshend, C. DiMiceli, M. Carroll, J. C. Eastman, M. Hansen, and R. S. DeFries (2002), Detection of land cover changes using MODIS 250m data, *Remote Sens. Environ.*, *83*, 336–350.

S. Gopal, K. Lo, R. B. Myneni, and N. V. Shabanov, Department of Geography, Boston University, 675 Commonwealth Avenue, Boston, MA 02215, USA. (shabanov@bu.edu)

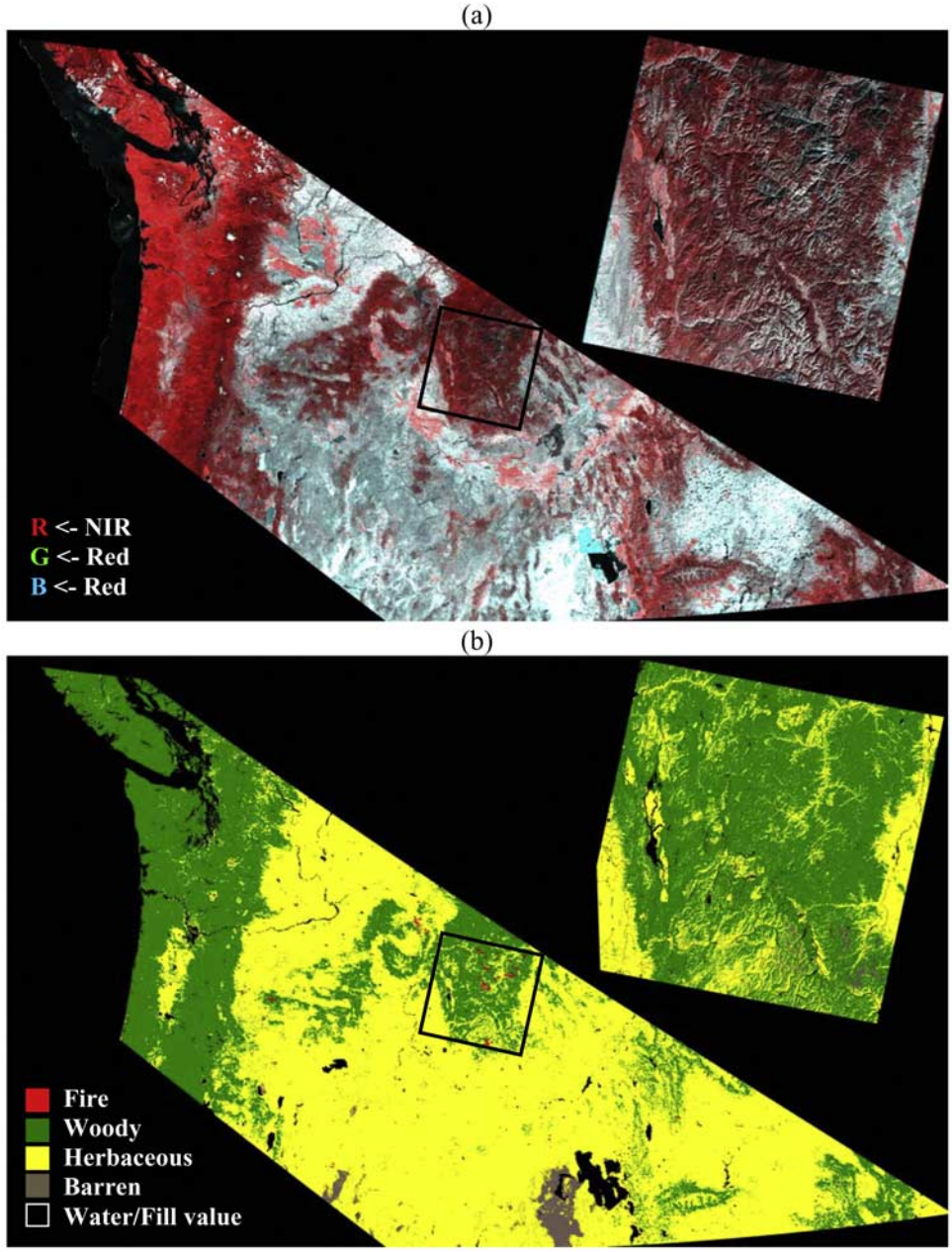

Figure 1. Input data for burn detection with the ARTMAP neural network. (a) The Moderate Resolution Imaging Spectroradiometer (MODIS) 8-day composite surface reflectance product at 500-m spatial resolution for 5–12 September 2000, tile h09v04 (h indicates horizontal; v indicates vertical), reprojected to the universal transverse Mercator (UTM) projection. (inset) Enhanced Thematic Mapper (ETM+) surface reflectance data at 30-m spatial resolution for 8 October 2000, path 41/row 29, the UTM projection. (b) The three vegetation life forms land cover for the above–MODIS tile overlaid with the composite (20 August to 12 September 2000) of MODIS fire product. (inset) Three vegetation life forms land cover for the ETM+ scene.

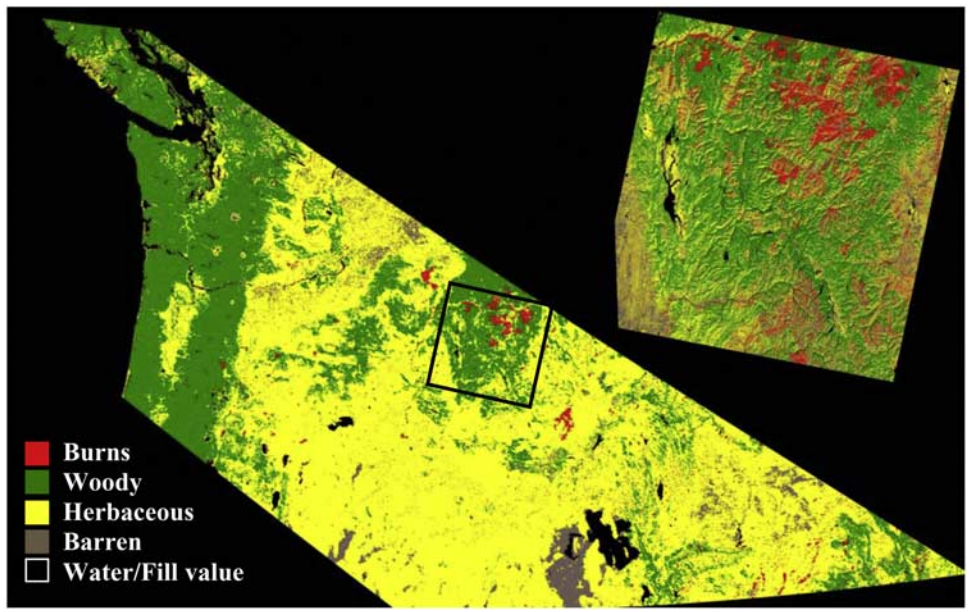

Figure 4. The ARTMAP discrete classification of the MODIS and the ETM+ surface reflectance data.